Multiple electronic Raman scatterings in a single metallic carbon nanotube

Daqi Zhang (张达奇),[1] Juan Yang (杨娟),[1,*] Eddwi H. Hasdeo,[2] Can Liu (刘灿),[3] Kaihui Liu (刘开辉),[3]
Riichiro Saito,[2] and Yan Li (李彦)[1,†]

[1]*Beijing National Laboratory for Molecular Sciences, Key Laboratory for the Physics and Chemistry of Nanodevices,*
State Key Laboratory of Rare Earth Materials Chemistry and Applications, College of Chemistry
and Molecular Engineering, Peking University, Beijing 100871, China
[2]*Department of Physics, Tohoku University, Sendai 980–8578, Japan*
[3]*State Key Laboratory for Mesoscopic Physics, Collaborative Innovation Center of Quantum Matter,*
School of Physics, Peking University, Beijing 100871, China

We observe multiple electronic Raman scatterings (ERSs) in a single suspended metallic single-walled carbon nanotube. The ERS process originates from the inelastic scattering of photoexcited excitons by a continuum of low-lying electron-hole pairs. In previous work, the observed Fano factor of the G band line shape is always negative; however, in this work we find that the Fano factor can be either positive or negative depending on the relative position of the nearest ERS with respect to the G band. This supports the idea that the origin of the G band asymmetry is an interference between the discrete G band and the continuous ERS. We also report that the ERS position and intensity are sensitive to the nanotube bundling effect and the laser heating effect.

I. INTRODUCTION

Single-walled carbon nanotubes (SWNTs) can be classified as either metallic or semiconducting tubes [1] depending on whether or not a cutting line [2], which is the one-dimensional Brillouin zone of a SWNT in the two-dimensional hexagonal Brillouin zone of a graphene, crosses the K point in the two-dimensional Brillouin zone. The electronic band structure of metallic tubes (M-SWNTs) differs from that of the semiconducting tubes (S-SWNTs) by the existence of a pair of linear subbands arising from the gapless dispersion near the K point and by the consequent low-energy electron-hole pairs across these subbands. The photoexcited excitons can be inelastically scattered by these low-lying electron-hole pairs and by phonons; these are known as electronic Raman scattering (ERS) and phonon Raman scattering processes, respectively. The phonon Raman spectra have been extensively studied [3,4] and widely used in SWNT characterization [5–10], whereas the ERS feature was recently discovered by Farhat *et al.* [11] and found to appear exclusively in M-SWNTs. The ERS process is a resonant enhancement process that occurs when the energy of a photon scattered by an electron-hole pair matches a corresponding excitonic transition energy ($M_{ii}, i = 1,2,3 \ldots$). Thus the ERS features are always centered at M_{ii}, and the energy of the scattered photons of ERS is independent of the excitation laser energy (E_L). Moreover, the ERS bands have a broad spectral linewidth ($\sim 500 \, \text{cm}^{-1}$), similar to that of electronic transitions, and are broader than phonon scattering peaks.

Farhat *et al.* [11] studied the ERS feature of M-SWNTs by Raman measurements using a tunable laser. By changing E_L, the combined Raman spectra of the phonon and ERS change as a function of E_L since the Stokes phonon Raman peaks appear at the energy $E_L - E_{\text{ph}}$, where E_{ph} is the phonon energy. These authors tuned E_L from slightly below M_{ii}^- to just above M_{ii}^+

and observed a single ERS feature corresponding to the nearest M_{ii} transition, which appears between the laser line and the G band ($\sim 1590 \, \text{cm}^{-1}$) feature, i.e., within 200 meV from E_L. Because all M-SWNTs, except for armchair tubes, have two split and closely spaced transition energies M_{ii}^+ and M_{ii}^- due to the trigonal warping effect [12], two separate ERS features that correspond to these two transition energies are expected. For M-SWNTs that have an M_{ii} more than 200 meV below E_L, in principle, it is also possible to observe the ERS features at a higher Raman shift than the G band.

Although the broad and asymmetric Breit-Wigner-Fano (BWF) line shape of the G band has long been recognized as a hallmark to distinguish M-SWNTs from S-SWNTs, its nature is not yet fully understood. Some studies suggest that the BWF line shape originates from the interference between the discrete G band and the continuous ERS, with a negative Fano factor $1/q$ in the BWF line shape proportional to the coupling between the G band and ERS [13,14]. Some other studies explain it as the coupling of a collective excitation (plasmon) near the Fermi level with a phonon [15,16]. If the ERS feature can indeed be observed at a higher Raman shift than the G band, then how the G band line shape will be affected in such cases could help to clarify its nature.

In this work, we give experimental evidence that the ERS features can indeed appear at a higher Raman shift than the G band, and that the ERS^+ and ERS^- features can be observed simultaneously at M_{ii}^+ and M_{ii}^-, respectively. More importantly, we do obtain a positive (negative) value of $1/q$ in the BWF line shape of the G band when the ERS is observed at a higher (lower) Raman shift than the G band, which supports that the G band asymmetry originates from an interference between the discrete G band and the continuous ERS. Environmental factors including the nanotube bundling effect and the laser heating effect on the ERS features are also discussed.

II. EXPERIMENT

SiO$_2$/Si wafers with open slits (typical width of 65 μm) were used as the substrate. Growth of SWNTs over the slits was

---

*Corresponding author: yang_juan@pku.edu.cn
†Corresponding author: yanli@pku.edu.cn

carried out by a catalytic chemical vapor deposition (CCVD) method at 950 °C [17]. Ethanol served as the carbon source and cobalt (II) acetate as the catalyst precursor.

Micro-Raman measurements were performed on a Horiba Jobin-Yvon LabRAM ARAMIS system equipped with three excitation lasers at 532 nm (2.33 eV), 633 nm (1.96 eV), and 785 nm (1.58 eV). The orientation of the nanotubes, which were aligned on the open slit within 15° in the direction of the gas flow, was set to be parallel to the laser polarization, which was checked by Raman mapping of the sample. Stokes Raman spectra were acquired with edge filters cutting at 100 cm^{-1}. A 600 grooves/mm grating was used, giving a spectral resolution better than 2 cm^{-1}. The laser power was controlled under 1 mW to avoid laser heating effect, unless higher laser powers were intentionally used for some experiments. The typical accumulation time was 200 s for each spectrum. All Raman spectra were corrected by subtracting the background signal collected at a blank slit. Transmission spectra were acquired using a polarization-based homodyne technique developed by Liu *et al.* [18].

III. RESULTS AND DISCUSSION

A. ERS features in a single suspended M-SWNT

In order to probe the intrinsic ERS features, we first focus on single suspended M-SWNTs grown over open slits to avoid any influence from the substrate or bundles. Figure 1(a) shows the transmission and Raman spectra of the same suspended SWNT. The transmission spectrum gives the excitonic transition energies of this tube, which are 1.82 eV for M_{11}^- and 1.96 eV for M_{11}^+. The chirality of this tube is

assigned to (13,7) by comparison to the atlas of suspended SWNT optical transition energies [19]. Since no other bands are observed in the transmission spectrum, this SWNT must be an individual tube rather than a bundle.

Raman spectra with excitations of both 633 nm ($E_L = 1.96$ eV) and 532 nm ($E_L = 2.33$ eV) are recorded. At 633 nm excitation, an asymmetric and broad G band indicates the metallic nature of this tube. The radial breathing mode (RBM) observed at 171 cm^{-1} agrees with the (13,7) assignment. In addition, a strong broadband at 1.82 eV [blue dotted lines in Fig. 1(a)] matches the M_{11}^- of this tube. The featureless tail overlapping with the RBM suggests that a broadband lies near the 1.96 eV laser line [11]. At 532 nm excitation, which itself is not in resonance with any M_{ii} of this tube, no RBM feature and only a weak G band are expected and indeed observed due to the nonresonant conditions. However, the overtones 2D and 2G as well as the combination band G+2D are strongly enhanced by resonance. Their line shapes are asymmetric. After peak deconvolution, two broadbands are located at 1.83 and 1.98 eV [blue dotted lines in Fig. 1(a)], which match the M_{11}^- and M_{11}^+ in the transmission spectrum, respectively. The uncertainty found in the ERS position is less than ±10 meV by consideration of the errors introduced by spectral resolution, random noise, and the uncertainty in peak deconvolution.

To ensure that these two broadbands can be attributed to the ERS$^-$ and ERS$^+$, we need to exclude all other possible origins, such as double resonance and additional combination phonon modes. The fact that these two broadbands are on different energy sides of the 2D band and its combination band G+2D rules out the possibility of double resonance [20,21]. To further exclude the possibility of other combination
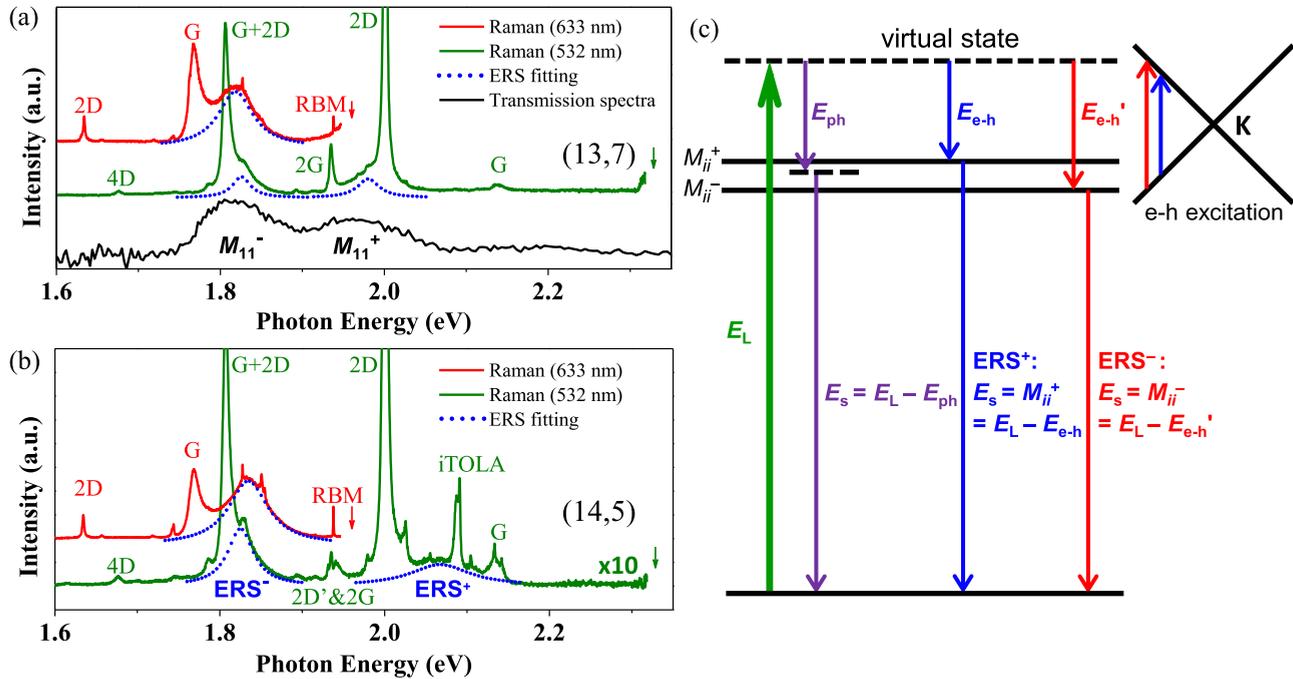
FIG. 1. Raman spectra (green for 532 nm excitation and red for 633 nm excitation) and transmission spectrum (black) of suspended M-SWNTs (a) (13,7) and (b) (14,5). The contributions of ERS$^+$ and ERS$^-$ (blue dotted lines) are fitted with a Lorentzian line shape. The arrows indicate the energies of the corresponding excitation laser lines. (c) Schematic of resonantly enhanced ERS$^+$ and ERS$^-$ processes in a M-SWNT, compared to a typical resonant Raman process. E_L, E_s, E_{ph}, and E_{e-h} represent the energies of laser, scattered photon, phonon mode, and electron-hole pair, respectively.

phonon modes, such as the 2D+RBM band, we use the Raman spectra of a (14,5) tube for comparison. (13,7) and (14,5) are two neighboring chiralities in the $2n + m = 33$ branch. As the difference in their diameters is less than 3%, the phonon energies of the two tubes are expected to be close. Although both chiralities have M_{11}^- at 1.82 eV, the M_{11}^+ of (14,5) at 2.04 eV is considerably higher than the 1.98 eV of (13,7) [19]. It is consistent with the trigonal warping effect that the energy separation between M_{11}^- and M_{11}^+ is larger for (14,5) with a smaller chiral angle than for (13,7) with a larger chiral angle in the same $2n + m$ branch [12]. Therefore, comparison between the Raman spectra of these two chiralities should tell whether the broadbands originate from the ERS features or from combination phonon modes.

The Raman spectra of (14,5) in Fig. 1(b) show similar phonon Raman peaks to those of (13,7) in the energy range of 1.6–1.9 eV, with a strong broadband at 1.83 eV. However, a dramatic difference lies in the energy range of 1.9–2.2 eV, in which a broadband at 2.06 eV can be deconvoluted for (14,5), and the combination mode of an in-plane transverse optical (iTO) phonon and a longitudinal acoustic (LA) phonon (iTOLA, $\sim 1900 \, \text{cm}^{-1}$) and the G band close to this broadband show significantly higher intensity than for (13,7). In addition, the disappearance of the broad tail overlapping with the RBM band at 633 nm excitation for (14,5) also indicates that the resonance band moves away from this laser line. All these data demonstrate that the origin of these two broadbands is from ERS$^-$ and ERS$^+$, respectively.

Figure 1(c) shows a schematic diagram of the ERS$^-$ and ERS$^+$ processes in an M-SWNT, compared to a typical resonant Raman process. In the ERS processes, the inelastic scattering of photoexcited excitons by low-energy electron-hole pairs is resonantly enhanced when the scattered photon energy (E_s) matches M_{ii}^- or M_{ii}^+, giving multiple ERS bands. In the resonant Raman process, there are two possible resonance conditions: (1) the incident photon energy is matched to the energy separation of real electronic states (incident resonance condition) and (2) the scattered photon energy is matched to the energy separation (scattered resonance condition) [4]. When the energy of a scattered photon is close to M_{ii} the scattered resonance condition is met, resulting in significantly enhanced Raman intensity for the corresponding phonon mode. This scattered resonance condition explains the unusually large intensity of the G+2D, 2D, iTOLA, and G modes in Figs. 1(a) and 1(b).

In this case, we not only observe the ERS features located as far as $\sim 500 \, \text{meV}$ (or $\sim 4000 \, \text{cm}^{-1}$) away from the laser line, but also simultaneously observe ERS$^+$ and ERS$^-$ at M_{ii}^+ and M_{ii}^-, respectively. Due to the resonant nature of ERS, the M_{ii}'s of M-SWNTs can be directly measured. Together with diameter measurements from the RBM frequency, in principle, accurate assignments of all M-SWNTs can be achieved solely using a standard micro-Raman spectrometer equipped with several discrete laser lines. A systematic work on this issue will be presented elsewhere.

B. Bundling effect on the ERS features

Next, we would like to study the influence of nanotube bundling effect on the ERS features, given that the van der
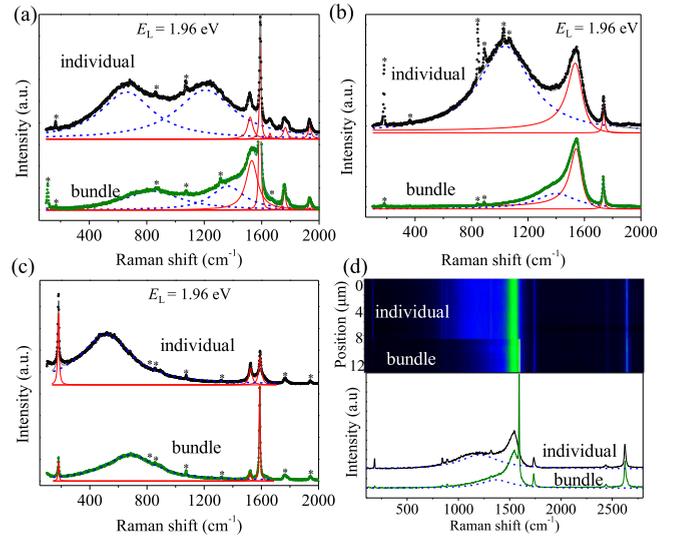
FIG. 2. Raman spectra of Y-shaped M-SWNTs (a) (12,9), (b) (15,3), and (c) (11,8) before (top) and after (bottom) bundling. The experimental spectra are given as open dots. Blue dashed lines show the fitted ERS bands, and the red solid lines are for the phonon modes. Peaks with asterisks are not included in the fitting. (d) Raman mapping and spectra of the same M-SWNT before and after bundling. The mapping data are acquired every 2 μm.

Waals interaction between bundled SWNTs can affect their M_{ii}'s as well as their phonon frequencies [22–25]. Y-shaped bundles suspended over slits were selected for study so that the individual part and the bundled part of the very same tube could be characterized and compared. The Y-shaped bundles typically consist of 2–4 SWNTs.

Figure 2(a) shows the Raman spectra of a Y-shaped bundle with an individual M-SWNT before and after bundling to another tube. At 1.96 eV excitation, the RBM of this M-SWNT is observed at 166 cm^{-1} for the individual tube, but shifts to 168 cm^{-1} upon bundling, whereas the RBM of the other tube is observed at 111 cm^{-1} in the bundled part. Before bundling, two broad and intense ERS bands appear at 658 cm^{-1} (0.08 eV) and 1209 cm^{-1} (0.15 eV). With $E_L = 1.96$ eV, we obtain the corresponding $M_{11}^+ = 1.96 - 0.08 = 1.88$ eV and $M_{11}^- = 1.96 - 0.15 = 1.81$ eV. The chirality of this M-SWNT can thus be assigned to (12,9) unambiguously. Several weak and sharp peaks marked by asterisks on top of the ERS bands are the intermediate-frequency modes (IFMs) [26–28]. For the bundled part, the corresponding ERS bands appear at 820 and 1388 cm^{-1}, indicating redshifts of 20 meV for M_{11}^+ and 22 meV for M_{11}^-. Figures 2(b) and 2(c) present the Raman spectra of Y-shaped individual and bundles of (15,3) and (11,8), respectively. The magnitudes of redshifts are all within the range of 20–56 meV reported by Wang *et al.* [22] using Rayleigh scattering spectroscopy for suspended SWNTs. The Raman measurements allow variations in phonon Raman modes to be studied in addition to the M_{ii} shifts. The Raman intensity change of various phonon modes can be explained by the scattered resonance condition. As the ERS band redshifts upon bundling, M_{ii} moves away from the RBM-scattered photon energy. Consequently, the RBM is in a less scattered-resonance condition with M_{ii}, resulting in

decreased RBM intensity. The intensities of the other weak phonon modes also decrease (increase) as M_{ii} moves away from (approaches) the phonon-scattered photon energy. On the other hand, the intensity of the ERS itself decreases upon bundling because of a reduced Coulomb interaction resulting from an increase in the environmental dielectric constant. Note that almost identical Raman spectra are observed at different positions of the bundled part [Fig. 2(d)]; therefore, the changes in Raman spectra are indeed caused by bundling, not by other environmental effects such as gas adsorption or amorphous carbon coating [25,29].

C. BWF line shape G band with regard to the ERS features

As discussed earlier, although the broad and asymmetric BWF line shape of the G band is a well-accepted hallmark to distinguish M-SWNTs from S-SWNTs, its origin remains a topic under debate. The BWF line shape can be written as

$$I(\omega) = I_0 \frac{[1 + 2(\omega - \omega_0)/q\Gamma]^2}{1 + [2(\omega - \omega_0)/\Gamma]^2}, \tag{1}$$

where ω_0, I_0, and Γ are fitting parameters for the central frequency, the intensity, and the broadening factor, respectively, whereas $1/q$ is the Fano factor that measures the asymmetry of the band [15]. When $1/q \to 0$, a Lorentzian line shape is recovered. The magnitude of $1/q$ depends on the chiral angle of the SWNT [30] and can be affected by local environments [31–36]. As we have demonstrated that the ERS bands can appear at a higher Raman shift than the G band, how the BWF line shape will be affected in such cases could help to clarify its nature.

Figure 3 shows the experimental and calculated Raman spectra of the individual and bundled parts of an M-SWNT with an ERS feature close to the G band. This M-SWNT can be assigned unambiguously to (17,5) according to the RBM frequency at $154\,\mathrm{cm}^{-1}$ and the transmission spectrum ($M_{11}^- = 1.59$ eV and $M_{11}^+ = 1.77$ eV) on the individual part. The calculated exciton energies $M_{11}^- = 1.60$ eV and $M_{11}^+ = 1.82$ eV are obtained by solving the Bethe-Salpeter equation using an extended tight-binding method [37] with an environmental dielectric constant $\kappa = 2.4$ [38]. In Fig. 3(a), peak deconvolution of the experimental spectrum gives a broad ERS$^+$ band centered at $1425\,\mathrm{cm}^{-1}$ by fitting the G band with a Lorentzian G$^+$ at $1594\,\mathrm{cm}^{-1}$ and a BWF line shape G$^-$ with $1/q = -0.19$. For the bundled part, an additional RBM at $121\,\mathrm{cm}^{-1}$ appears at 1.96 eV excitation, suggesting that an S-SWNT is involved. However, we can still be sure that the (17,5) tube exists in the bundle by considering the unshifted RBM at $154\,\mathrm{cm}^{-1}$ at 1.58 eV excitation and the nearly identical high-energy phonon modes above $2300\,\mathrm{cm}^{-1}$. The increased intensity of the M and iTOLA bands indicates that the ERS$^+$ has shifted to a higher Raman shift than the G band. Peak deconvolution of the spectra in the range of 1000–$2300\,\mathrm{cm}^{-1}$ [Fig. 3(b)] gives a broad ERS$^+$ band centered at $1778\,\mathrm{cm}^{-1}$, which is redshifted by 44 meV from that of the individual part. This redshift can be understood by an increase in the environmental dielectric constant due to bundling. Setting $\kappa = 4.0$, we obtain $M_{11}^- = 1.55$ eV and $M_{11}^+ = 1.75$ eV for bundled (17,5) [Fig. 3(c)]. More importantly, the fitting with a BWF line shape G$^-$ band gives rise to a positive $1/q$
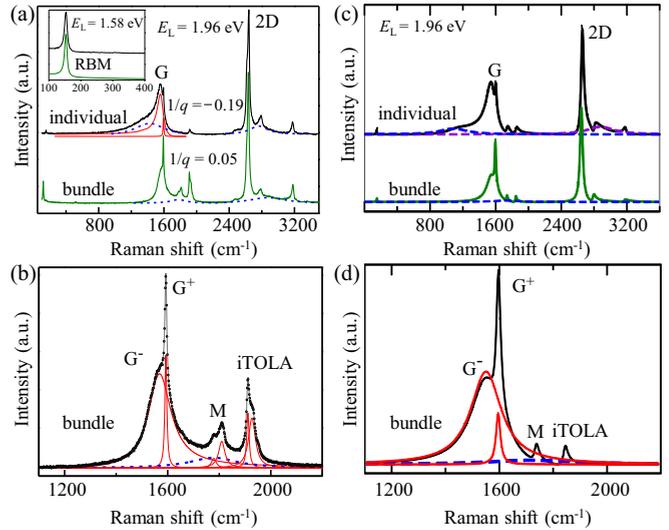
FIG. 3. (a) Raman spectra of a (17,5) tube before (top) and after (bottom) bundling at 1.96 eV excitation. The RBM at $121\,\mathrm{cm}^{-1}$ for the bundled part belongs to another S-SWNT. The inset shows the RBM of (17,5) at $154\,\mathrm{cm}^{-1}$ at 1.58 eV excitation. (b) The enlarged Raman spectrum for the bundled part in (a) and peak deconvolution. The experimental spectra are given as open dots. Blue dashed lines show the fitted ERS bands, red solid lines are for the phonon modes, and gray solid lines are the summation spectra of all fitted peaks. The G$^-$ band is fitted with a BWF line shape with a positive asymmetric Fano factor $1/q$ of 0.05, in contrast to a negative $1/q$ of -0.19 for the individual part. (c) Calculated Raman spectra of (17,5) at 1.96 eV excitation, obtained by setting the environmental dielectric constant κ as 2.4 for the individual part (top) and 4.0 for the bundled part (bottom). (d) The enlarged calculated Raman spectrum corresponding to that in (b). The calculated total Raman spectrum (black line) consists of the G$^+$ and G$^-$ bands (red lines, when ERS is set to 0) and the ERS band (blue dashed line).

value of 0.05. A positive (negative) $1/q$ value when the ERS feature is located at a higher (lower) Raman shift than the G band is a strong indication that the G band asymmetry originates from the interference between the discrete G band and the continuous ERS. In Fig. 3(d), the calculated ERS ($\sim 1780\,\mathrm{cm}^{-1}$) intensity is about one order of magnitude smaller than the G band. Nevertheless, the presence of ERS gives rise to the asymmetric line shape of the G band. The red lines in Fig. 3(d) are calculated spectra for the G$^+$ and G$^-$ bands, respectively, when the ERS intensity is set to zero. Doping and strain effects upon bundling can be excluded based on the unshifted RBM and 2D frequencies [39–41]. We want to point out that the fitting can be affected by the large contributions of M and iTOLA bands. Although it is also possible to fit the spectra by only Lorentzian peaks, fitting with a BWF line shape by imposing the requirement for $1/q$ to be negative fails undoubtedly.

D. Laser heating effect on the ERS features

As the transition energies of a SWNT can be perturbed by heating [42,43], we would like to further explore how the ERS feature and its interference with the G band change upon laser heating. Figure 4(a) shows the Raman spectra
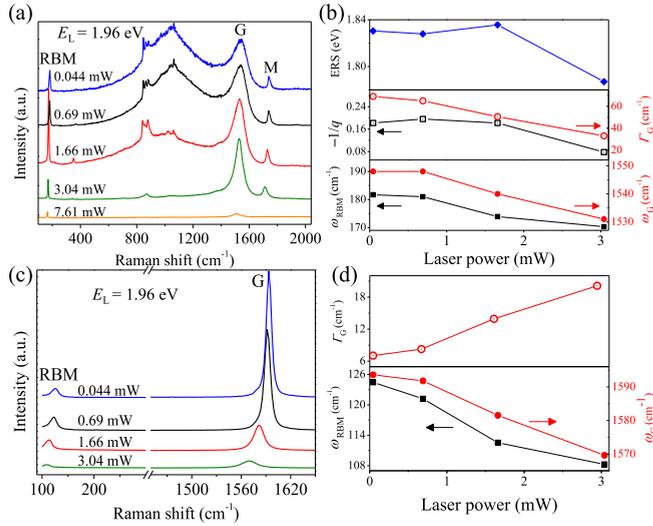
FIG. 4. (a) Raman spectra of a (16,1) tube at different excitation laser powers. (b) The ERS position (top), $-1/q$ and Γ_G (middle), and the Raman shifts of RBM and G band (bottom) of (16,1) as functions of the laser power. (c) Raman spectra of a S-SWNT at different excitation laser powers. (d) Γ_G (top) and Raman shifts of RBM and G band (bottom) for this S-SWNT as a function of the laser power.

provides further evidence to support the idea that the BWF asymmetry of the G^- band originates from the interference between the G band and ERS. Moreover, the ERS feature disappears before the phonon Raman peaks do upon heating. Thermal-induced electron occupation in the conduction band inhibits interband transition of the electron due to the Pauli blocking, and consequently the ERS is suppressed.

Normally, peak broadening is expected upon heating, as is observed for the M feature [Fig. 4(a)] and for an S-SWNT sample [Figs. 4(c) and 4(d)]. However, both the G band and the RBM of this M-SWNT become narrower with increasing laser power [Fig. 4(b)]. This supports the idea that the origin of the broadening of the RBM and G band is due to the interband transition of the electron by means of the electron-phonon interaction (the Kohn anomaly effect) [46]. Similarly to the suppression of ERS upon heating, the Kohn anomaly effect is also suppressed because of the Pauli blocking, resulting in a sharper RBM and G band.

IV. CONCLUSIONS

In this work, we have shown that by utilizing a standard micro-Raman spectrometer equipped with several discrete laser lines, the ERS^+ and ERS^- features of M-SWNTs can be observed simultaneously at the corresponding M_{ii}^+ and M_{11}^-. We have observed the ERS features at a higher Raman shift than the G band, and, consequently, have obtained a positive value of the Fano factor $1/q$ in the BWF line shape G band. Our data support the idea that the nature of the G band asymmetry originates from the interference between the discrete G band and the continuous ERS. In addition, we have also observed the ERS features in SWNT bundles and found that the ERS bands redshift upon bundling. Upon heating, the ERS band first blueshifts due to gas desorption on the SWNT walls and then redshifts because of thermal expansion of SWNT and the consequently redshifted transition energies. The ERS intensity decreases upon both bundling and heating.

of a M-SWNT acquired at different laser powers ranging from 0.044 to 7.61 mW, with all intensities normalized to the $521\,\text{cm}^{-1}$ Si peak on the substrate. Based on the RBM frequency at $181\,\text{cm}^{-1}$ and ERS^- at 1.83 eV, this tube is assigned as (16,1). At laser powers below 1 mW, the two spectra are similar, indicating a negligible laser heating effect. At laser powers higher than 1 mW, downshifts in the RBM and G band, as well as the M band ($\sim 1750\,\text{cm}^{-1}$), can be observed, which are widely reported as the results of laser heating [44]. Upon heating, the ERS band first blueshifts (at 1.66 mW laser power) and then redshifts [at 3.04 mW laser power; top panel in Fig. 4(b)]. Such behavior in transition energies was also reported previously for the photoluminescence (PL) spectra of S-SWNTs during thermal heating [45]. The initial blueshift comes from the desorption of gas molecules on SWNT walls, which occurs fast at low temperatures ($<100\,^\circ$C) [45]. Further increase in temperature leads to thermal expansion of SWNTs and redshifted transition energies [43]. Upon heating, the ERS intensity decreases continuously while a general decreasing trend is observed for the value of $-1/q$. This

[1] R. Saito, M. Fujita, G. Dresselhaus, and M. S. Dresselhaus, Appl. Phys. Lett. **60**, 2204 (1992).

[2] G. G. Samsonidze, R. Saito, A. Jorio, M. A. Pimenta, A. G. Souza Filho, A. Gruneis, G. Dresselhaus, and M. S. Dresselhaus, J. Nanosci. Nanotechnol. **3**, 431 (2003).

[3] M. S. Dresselhaus, A. Jorio, and R. Saito, Annu. Rev. Condens. Matter Phys. **1**, 89 (2010).

[4] R. Saito, M. Hofmann, G. Dresselhaus, A. Jorio, and M. S. Dresselhaus, Adv. Phys. **60**, 413 (2011).

[5] A. Jorio, A. P. Santos, H. B. Ribeiro, C. Fantini, M. Souza, J. P. M. Vieira, C. A. Furtado, J. Jiang, R. Saito, L. Balzano *et al.*, Phys. Rev. B **72**, 075207 (2005).

[6] P. T. Araujo, S. K. Doorn, S. Kilina, S. Tretiak, E. Einarsson, S. Maruyama, H. Chacham, M. A. Pimenta, and A. Jorio, Phys. Rev. Lett. **98**, 067401 (2007).

[7] T. Michel, M. Paillet, D. Nakabayashi, M. Picher, V. Jourdain, J. C. Meyer, A. A. Zahab, and J. L. Sauvajol, Phys. Rev. B **80**, 245416 (2009).

[8] D. Zhang, J. Yang, F. Yang, R. Li, M. Li, D. Ji, and Y. Li, Nanoscale **7**, 10719 (2015).

[9] D. Zhang, J. Yang, and Y. Li, Small **9**, 1284 (2013).

[10] Q. Zhao and J. Zhang, Small **10**, 4586 (2014).

[11] H. Farhat, S. Berciaud, M. Kalbac, R. Saito, T. F. Heinz, M. S. Dresselhaus, and J. Kong, Phys. Rev. Lett. **107**, 157401 (2011).

[12] R. Saito, G. Dresselhaus, and M. S. Dresselhaus, Phys. Rev. B **61**, 2981 (2000).

[13] E. H. Hasdeo, A. R. T. Nugraha, K. Sato, M. S. Dresselhaus, and R. Saito, Phys. Rev. B **88**, 115107 (2013).

[14] R. Saito, K. Sato, P. T. Araujo, D. L. Mafra, and M. S. Dresselhaus, Solid State Commun. **175-176**, 18 (2013).

[15] S. D. M. Brown, A. Jorio, P. Corio, M. S. Dresselhaus, G. Dresselhaus, R. Saito, and K. Kneipp, Phys. Rev. B **63**, 155414 (2001).

[16] C. Jiang, K. Kempa, J. Zhao, U. Schlecht, U. Kolb, T. Basché, M. Burghard, and A. Mews, Phys. Rev. B **66**, 161404 (2002).

[17] W. Zhou, Z. Han, J. Wang, Y. Zhang, Z. Jin, X. Sun, Y. Zhang, C. Yan, and Y. Li, Nano Lett. **6**, 2987 (2006).

[18] K. Liu, X. Hong, S. Choi, C. Jin, R. B. Capaz, J. Kim, W. Wang, X. Bai, S. G. Louie, E. Wang *et al.*, Proc. Natl. Acad. Sci. USA **111**, 7564 (2014).

[19] K. Liu, J. Deslippe, F. Xiao, R. B. Capaz, X. Hong, S. Aloni, A. Zettl, W. Wang, X. Bai, S. G. Louie *et al.*, Nat. Nanotechnol. **7**, 325 (2012).

[20] A. G. Souza Filho, A. Jorio, G. G. Samsonidze, G. Dresselhaus, M. S. Dresselhaus, A. K. Swan, M. S. Unlu, B. B. Goldberg, R. Saito, and J. H. Hafner, Chem. Phys. Lett. **354**, 62 (2002).

[21] A. G. Souza Filho, A. Jorio, A. K. Swan, M. S. Ünlü, B. B. Goldberg, R. Saito, J. H. Hafner, C. M. Lieber, M. A. Pimenta, and G. Dresselhaus *et al.*, Phys. Rev. B **65**, 085417 (2002).

[22] F. Wang, M. Y. Sfeir, L. Huang, X. M. Henry Huang, Y. Wu, J. Kim, J. Hone, S. O'Brien, L. E. Brus, and T. F. Heinz, Phys. Rev. Lett. **96**, 167401 (2006).

[23] Z. Luo, F. Papadimitrakopoulos, and S. K. Doorn, Phys. Rev. B **77**, 035421 (2008).

[24] N. Peica, C. Thomsen, and J. Maultzsch, Nanoscale Res. Lett. **6**, 174 (2011).

[25] S. Chiashi, K. Kono, D. Matsumoto, J. Shitaba, N. Homma, A. Beniya, T. Yamamoto, and Y. Homma, Phys. Rev. B **91**, 155415 (2015).

[26] C. Fantini, A. Jorio, M. Souza, R. Saito, G. G. Samsonidze, M. S. Dresselhaus, and M. A. Pimenta, Phys. Rev. B **72**, 085446 (2005).

[27] Z. Luo, F. Papadimitrakopoulos, and S. Doorn, Phys. Rev. B **75**, 205438 (2007).

[28] J. Wang, J. Yang, D. Zhang, and Y. Li, J. Phys. Chem. C **116**, 23826 (2012).

[29] D. Levshov, T. X. Than, R. Arenal, V. N. Popov, R. Parret, M. Paillet, V. Jourdain, A. A. Zahab, T. Michel, Y. I. Yuzyuk *et al.*, Nano Lett. **11**, 4800 (2011).

[30] Y. Wu, J. Maultzsch, E. Knoesel, B. Chandra, M. Huang, M. Y. Sfeir, L. E. Brus, J. Hone, and T. F. Heinz, Phys. Rev. Lett. **99**, 027402 (2007).

[31] M. Paillet, P. Poncharal, A. Zahab, J. L. Sauvajol, J. C. Meyer, and S. Roth, Phys. Rev. Lett. **94**, 237401 (2005).

[32] K. T. Nguyen, A. Gaur, and M. Shim, Phys. Rev. Lett. **98**, 145504 (2007).

[33] M. Shim, A. Gaur, K. T. Nguyen, D. Abdula, and T. Ozel, J. Phys. Chem. C **112**, 13017 (2008).

[34] A. Gaur and M. Shim, Phys. Rev. B **78**, 125422 (2008).

[35] B. Hatting, S. Heeg, K. Ataka, J. Heberle, F. Hennrich, M. M. Kappes, R. Krupke, and S. Reich, Phys. Rev. B **87**, 165442 (2013).

[36] B. Hatting, S. Heeg, and S. Reich, Phys. Status Solidi B **250**, 2639 (2013).

[37] J. Jiang, R. Saito, G. G. Samsonidze, A. Jorio, S. G. Chou, G. Dresselhaus, and M. S. Dresselhaus, Phys. Rev. B **75**, 035407 (2007).

[38] A. R. T. Nugraha, R. Saito, K. Sato, P. T. Araujo, A. Jorio, and M. S. Dresselhaus, Appl. Phys. Lett. **97**, 091905 (2010).

[39] K.-i. Sasaki, R. Saito, G. Dresselhaus, M. S. Dresselhaus, H. Farhat, and J. Kong, Phys. Rev. B **78**, 235405 (2008).

[40] H. Farhat, K. Sasaki, M. Kalbac, M. Hofmann, R. Saito, M. S. Dresselhaus, and J. Kong, Phys. Rev. Lett. **102**, 126804 (2009).

[41] M. Kalbac, L. Kavan, H. Farhat, J. Kong, and M. S. Dresselhaus, J. Phys. Chem. C **113**, 1751 (2009).

[42] S. B. Cronin, Y. Yin, A. Walsh, R. B. Capaz, A. Stolyarov, P. Tangney, M. L. Cohen, S. G. Louie, A. K. Swan, M. S. Unlu *et al.*, Phys. Rev. Lett. **96**, 127403 (2006).

[43] P. May, H. Telg, G. Zhong, J. Robertson, C. Thomsen, and J. Maultzsch, Phys. Rev. B **82**, 195412 (2010).

[44] Y. Zhang, H. Son, J. Zhang, J. Kong, and Z. Liu, J. Phys. Chem. C **111**, 1988 (2007).

[45] P. Finnie, Y. Homma, and J. Lefebvre, Phys. Rev. Lett. **94**, 247401 (2005).

[46] K.-i. Sasaki, H. Farhat, R. Saito, and M. S. Dresselhaus, Physica E **42**, 2005 (2010).